Contrib Mineral Petrol (2001) 141: 174–185
DOI 10.1007/s004100000217

W. J. Dunlap · A. K. Kronenberg

Argon loss during deformation of micas: constraints from laboratory deformation experiments

Received: 12 October 1999 / Accepted: 3 October 2000 / Published online: 16 March 2001

Abstract The role of internal deformation in resetting argon ages of micas has been investigated by measuring $^{40}Ar/^{39}Ar$ ratios of biotite and muscovite, before and after experimentally deforming them. Neither mica crushed cataclastically at room temperature on-line with a mass spectrometer showed any measurable change in $^{40}Ar/^{39}Ar$ age. Muscovite crystals either sheared along the K-interlayer and/or kinked at 400 °C and 100–200 MPa confining pressure, exhibit small (0.7–1.0%) reductions in age and marked increases in bulk diffusion coefficients, as determined from argon release during the initial stages of step-heating between 550 and 810 °C. We conclude that the relatively young ages of fine-grained mica populations in naturally deformed mylonites result primarily from grain size refinement and reductions in length scale for volume diffusion and/or by syntectonic neocrystallization. Internal deformation involving dislocation slip and kinking may contribute to some argon loss by pipe diffusion, but reductions in closure temperature associated with multipath diffusion are small.

Supplementary material for this paper can be obtained electronically by using the Springer LINK server located at http://dx.doi.org/10.1007/s004100000217.

W. J. Dunlap (✉)[1]
UCLA, Department of Earth and Space Sciences,
Los Angeles, CA 90024, USA
E-mail: jim.dunlap@anu.edu.au

A. K. Kronenberg
Center for Tectonophysics, Department of Geology
and Geophysics, Texas A&M University,
College Station, TX 77843-3113, USA

Present address:
[1]Research School of Earth Sciences, The Australian
National University, Canberra, ACT, 0200 Australia

Editorial responsibility: K.V. Hodges

Introduction

Internal deformation of micas under greenschist facies conditions is suspected of inducing or enhancing argon loss, with the effect of erasing or obscuring age information for events prior to deformation, and providing a means, in specialized cases, of dating the deformation (e.g., Dunlap et al. 1991). Positive correlations between physical grain size and bulk age observed for micas from mylonites are commonly attributed to either combined syntectonic grain size reduction and subsequent volume diffusional loss of argon, or to the growth of fine neocrystallized grains during deformation and the development of two generations of mica in the same rock. However, it is difficult to rule out that the smallest grains in mylonites are younger because they have experienced more internal deformation, and that this deformation has resulted in greater loss of accumulated radiogenic argon.

$^{40}Ar/^{39}Ar$ ages of mica aggregates from highly deformed, greenschist facies rocks are difficult to interpret because such mica populations (e.g., Fig. 1) are not generally homogeneous (e.g., Kligfield et al. 1986). Micas are weak at low temperatures relative to the strengths of other rock-forming silicates and they may be actively deformed while they cool through the closure window for argon retention (Kelley 1988; Dunlap 1997). Thus, although micas undergo closure, they may also be undergoing internal strain by dislocation slip, some grains may be dissolving (perhaps completely) while new mica grains may be growing (Dunlap et al. 1991; West and Lux 1993), grain sizes may be decreasing because of strain-related segmentation (e.g., Goodwin and Renne 1991), and the stoichiometry of grains may be changing through time (e.g., Scaillet et al. 1992; Hames and Cheney 1997). Some or all of these processes may conspire to determine the final argon concentration that we measure in the laboratory.

One of the most poorly understood of the above effects is internal deformation of micas. Ages of fine-grained micas are commonly younger in deformed rocks

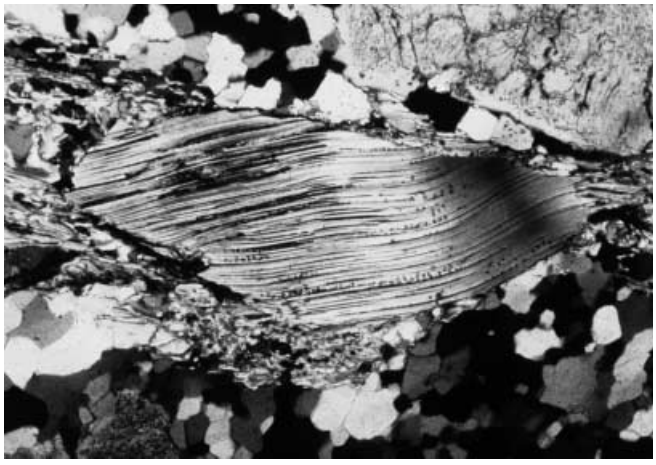

Fig. 1 Photomicrograph of porphyroclast of muscovite sheared along the basal plane under greenschist facies conditions (sample 796 of Dunlap 1997), long dimension ~1.5 mm. Deformation of the porphyroclast is predominantly by dislocation glide within the cleavage plane, resulting in the undulatory extinction, but there is some evidence for the operation of additional deformation mechanisms, including kinking and cracking (resulting in the finer grains that appear to be torn away from the porphyroclast), and possibly cataclasis and chemical alteration between cleavages (resulting in the darker amorphous zones). Neocrystallized mica has also formed in the fine grained groundmass (Dunlap 1997)

than those of coarse micas, and syntectonic grain size reduction by dynamic recrystallization and neocrystallization provide clear means of obtaining young argon ages by reducing length scales for volume diffusion; argon may be released to mobile grain boundaries and it may be excluded from new grains, respectively, during recrystallization and neocrystallization (Kligfield et al. 1986; Kelley 1988; Dunlap et al. 1991; Goodwin and Renne 1991; Hames and Bowring 1994; Dunlap 1997; Reddy and Potts 1999). In contrast, we know little about the direct effects of deformation. We do not know whether deformation decreases the ability of a mica grain to retain radiogenic argon, nor do we know anything about argon partitioning at dislocations or rates of pipe diffusion along dislocations.

Micas deform by a variety of mechanisms under greenschist facies conditions (e.g., Wilson and Bell 1979). Common deformation mechanisms include (1) kinking during cleavage-parallel shortening and associated segmentation by the introduction of dilatant kink band boundaries (Etheridge et al. 1973; Bell et al. 1986; Shea and Kronenberg 1992; Christoffersen and Kronenberg 1993), (2) cracking and separation along cleavage surfaces under a wide range of low normal stress states (Obreimoff 1930; Leonesio 1968; Goodwin and Wenk 1990), (3) cracking across cleavage (Goodwin and Wenk 1990; Mares and Kronenberg 1993) during bending or cleavage-parallel extension, and (4) intracrystalline plastic deformation via dislocation slip (or glide) within the K-interlayer (i.e., within the cleavage) in response to shear stresses resolved on cleavage (Demny 1963; Bell and Wilson 1981; Banos et al. 1983; Meike 1989; Christoffersen and Kronenberg 1993; Mares and Kronenberg 1993). Mechanisms (1) and (3) shorten diffusion length scales, thereby enhancing diffusive argon loss by providing shorter pathways, whereas mechanism (2) should not have an effect if diffusion of argon is parallel to cleavage. Rather than changing length scales, dislocations introduced during deformation (mechanism 4) may provide rapid, short-circuit diffusional paths (in parallel with lattice diffusion) between grain interiors and grain boundaries (e.g., Lee 1995).

In this paper the relationship between deformation of mica and argon loss is examined through experiments in which micas with large radiogenic argon contents are deformed and mass spectrometry is used to determine the amount of argon loss, either during or after the deformation experiments. Two cases are examined in detail, (1) cataclastic (brittle) deformation of biotite, involving cracking and brittle grain refinement, in addition to some dislocation glide, by crushing specimens on-line with a mass spectrometer, and (2) intracrystalline glide and kinking of muscovite with little or no cracking induced at elevated pressure and temperature in a triaxial gas-medium deformation apparatus (samples of Mares and Kronenberg 1993).

Background

Basal dislocation slip within the K-interlayer of micas (e.g., Banos et al. 1983) has been activated experimentally at temperatures as low as 20 °C and as high as 800 °C (Borg and Handin 1966; Etheridge et al. 1973; Meike 1989; Kronenberg et al. 1990, 1992; Mares and Kronenberg 1993; Noe et al. 1999). Dislocations have been imaged (at densities of $\sim 10^6$ mm^{-2}) within the basal plane in micas deformed in nature (e.g., Bell et al. 1986) with the same slip vectors as activated in experiments. Optical undulatory extinction of micas (Wilson and Bell 1979; Wilson 1980; Behrmann 1984; Lister and Snoke 1984; Dunlap et al. 1995) is evident in rocks deformed over a range of pressure and temperature conditions, from the very low grade environments that generally lead to cataclasis, to the high-grade environments (i.e., amphibolite facies) that lead to ductile shear and crystal plasticity. Recrystallization tends to remove the evidence for dislocation slip in micas of high grade rocks, yet mica porphyroclasts that have escaped recrystallization during greenschist facies deformations (Fig. 1) offer dramatic examples of external rotations caused by basal slip. If argon loss from micas is significantly enhanced by the introduction and glide of dislocations, then the deformation process could have a profound, direct effect on $^{40}Ar/^{39}Ar$ geochronology because it operates below temperatures where closure to volume diffusion of argon takes place ($< \sim 300$ °C; Dodson 1973).

A case has been made that diffusive loss of argon from micas is predominantly parallel to the cleavage (i.e., in the K-interlayer), and that the characteristic diffusion dimension is the physical radius of the crystal measured within the basal plane (Hames and Bowring

1994), or some significant fraction of this distance (Dunlap 1997). It follows that fragmentation of micas during deformation, with consequent decreases in cleavage-parallel diffusion distances, results in decreased retention of radiogenic argon within grain interiors. Detailed studies of mica populations in mylonite zones have generally supported this interpretation (e.g., Goodwin and Renne 1991).

Deformed and recrystallized micas of the Arltunga nappe complex of central Australia (Fig. 1) dated by Dunlap et al. (1995) using the $^{40}Ar/^{39}Ar$ method (their Fig. 4) show a remarkably wide range of apparent ages. The age spectra for aggregates of the course porphyroclasts generally rise over the course of step-heating experiments by as much as 1 Ga. Dunlap et al. (1995) interpreted these age gradients to reflect partial argon loss from Proterozoic igneous micas brought about mostly by late Paleozoic reheating, but also by minor recrystallization. However, the relict igneous grains (large grain in Fig. 1) were pervasively deformed by dislocation slip in the Paleozoic, leading to the characteristic textures shown in Fig. 1, and the effect of this internal deformation on argon retention remains unclear.

Hames and Cheney (1997) considered the possible causes of Paleozoic deformation-related argon loss from Proterozoic muscovite of the Green Mountain massif, Vermont. They suggested that, for brief Paleozoic overprinting events at ~425 °C, diffusive loss of argon played a subordinate role to a combination of chemically-induced and deformation-induced loss of argon. They concluded that chemical alteration and deformation can result in loss of accumulated ^{40}Ar, but they had no means of addressing whether deformation alone might enhance argon loss.

Kligfield et al. (1986), Kelley (1988), and Goodwin and Renne (1991) noted dramatic grain size effects in micas deformed over the sub-greenschist to amphibolite facies range of conditions. Smaller grain sizes generally recorded younger K–Ar and $^{40}Ar/^{39}Ar$ ages and the preferred interpretations were that the smaller grains had lost more argon via volume diffusion. These authors have also speculated that intracrystalline deformation may have had an affect on the argon systematics, but they were unable to address this issue in any detail. In contrast, Itaya and Takasugi (1988) noted a lack of correlation between K–Ar ages and grain sizes of muscovites from greenschist to amphibolite facies Sanbagwa schists. In their case there is a clear correlation between the youngest ages and the lowest metamorphic grades. Their preferred interpretation was that the argon was depleted from the lower grade schists during late syn-metamorphic deformation at ~100–250 °C, the extent of the depletion depending on the severity of the deformation.

Only few studies have examined quantitatively the contributions of pipe diffusion along dislocations to net transport in silicates (Yund et al. 1981, 1989; Yurimoto et al. 1989, 1992), and we know of no measurements of argon pipe diffusion in any silicate. Nevertheless, there are good reasons to suspect that argon loss may be affected by the introduction and glide of dislocations. Attractive interactions in a wide variety of crystalline materials between point defects and dislocations lead to preferential partitioning of solute impurities within dislocation cores and to diffuse local solute concentrations, known as Cottrell atmospheres, surrounding the dislocations (Cottrell and Jaswon 1949; Friedel 1964; Ho and Pratt 1983; Chen 1984; Lee 1995; Gukasyan et al. 1996; Varschavsky and Donoso 1997). Once localized at dislocations, solutes may be transported parallel to the dislocation lines by pipe diffusion at rates that exceed those of solute diffusion through the lattice by many orders of magnitude (e.g., Hart 1957; Suprun 1982; Le Claire and Rabinovitch 1984; Arabczyk et al. 1988; Badrour et al. 1989; Shiryaev et al. 1989; Hara and Endo 1997; Estrin and Rabkin 1998). Net transport by pipe diffusion is particularly effective when dislocations are mobile because exchange of the diffusing species is enhanced between moving dislocations and the surrounding crystal, and because point defect concentration gradients along the lengths of dislocations are greater during slip than can be maintained within dislocations that are stationary (Ruoff and Balluffi 1963). Transport of solutes perpendicular to mobile dislocations may be enhanced in the direction of dislocation motion as solutes are swept up and segregated at the moving dislocations and as diffuse Cottrell atmospheres follow the mobile dislocations (Cottrell and Jaswon 1949; Friedel 1964).

Potential contributions of diffusion along dislocations and other high-diffusivity pathways to the loss of radiogenic isotopes from minerals and the implications for geochronology have been considered by Lee (1995). In the case of argon loss from micas undergoing dislocation slip, daughter ^{40}Ar impurities that initially occupy parent potassium sites may concentrate at dislocations by diffusion or by being swept up by mobile dislocations that glide within the potassium interlayer. If, as Lee (1995) suggests, pipe diffusion of argon is three to four orders of magnitude (or more) faster than volume diffusion through the lattice and argon partitions preferentially into dislocations, then we might expect greater argon loss from deformed micas than from undeformed micas. Alternatively, if pipe diffusion of argon is rapid compared with lattice diffusion and dislocations form a significant volume fraction of the mica (i.e., dislocations occur in high densities and/or their effective radii are large, corresponding to significant Cottrell atmospheres), then we may obtain the same result. However, until now there has been no experimental study that bears directly on this question.

Dating studies of experimentally deformed micas are lacking and the results that are available are inconclusive. Gusev et al. (1969) found that dry grinding of ~250 μm muscovite and phlogopite in a planetary ball mill induced an exponential decline in argon content of the micas to essentially zero concentration after ~10 min

of grinding. In the initial 1–2 min of grinding, argon loss was pronounced (> 50%), at the same time that infrared absorption spectra indicated little change in the structural state of the micas. In the initial stage of grinding, the micas were reduced to 1- to 10-μm fragments and they concluded that the argon loss was purely a result of "mechanical destruction". However, prolonged grinding appears to have resulted in transformation of the micas into other phases, most likely as a result of the generation of locally high temperatures during grinding. Thus, the significance of these results is unclear because thermal and mechanical processes may have been competing to release the argon. We are aware of only one other published attempt to release argon by mechanical disintegration, in which Hanson and Gast (1967) reduced the grain size of ~410 μm biotite using a mortar and pestle. In that study, grinding did not release any argon from the resultant 180-μm fragments (within a reported uncertainty of 4%).

Methods

A biotite, designated Fe-mica (cf. Grove and Harrison 1996), was irradiated to produce ^{39}Ar (a proxy for K) and an undeformed split was step-heated for comparison with the deformed material. A second split of the Fe-mica (5.50 mg; five grains) was crushed on-line with a mass spectrometer to measure the $^{40}Ar/^{39}Ar$ age of the released gas. The driving force on the crusher (a modified Varian minivalve; Harrison et al. 1993), applied through a torque wrench, was increased in steps up to 65 inch-pounds and the isotopic content of the gas evolved during each step was analyzed. Individual crushing steps took place ~1 h apart. The crushing experiments ended when the copper gasket on the assembly was overcome by the driving force (signified by a major air component in the analyzed gas). The temperature during slow crushing was probably within a few degrees of room temperature. We did not attempt to install a thermocouple, although we suspect that the thermal inertia of the plunger and base (several cubic centimeters of stainless steel) would have maintained the tiny micas to within a few degrees of room temperature. After crushing, the fragments were sieved into four size fractions, < 25, 25–75, 75–150, and > 150 μm for step-heating. The 75–150 μm fraction was not analyzed because no significant change in age was observed for the other three fractions.

Three muscovite samples cut from a single crystal (from Methuen Township, Ontario; Hurlbut 1956) and deformed in a triaxial deformation apparatus (Mares and Kronenberg 1993) were subsequently irradiated with neutrons and then analyzed for their argon isotopic content. Muscovite Sample M11 was deformed to 14% strain at 400 °C and a lateral confining pressure of 200 MPa by applying a differential compressive load at 45° to (001) to promote dislocation slip with shear taking place parallel to [310]. Sample M22 was shortened by 11% under similar conditions to those imposed on M-11, loading at 45° to (001), but with shear parallel to [110]. Sample M-48 was deformed by 11% at 400 °C and a confining pressure of 100 MPa, this time loading the specimen parallel to (001) and to [010] to promote kink band formation. None of these deformed muscovite samples contain recrystallized grains, subgrains, or finely crushed products of cataclasis.

Preparation of the muscovite samples for triaxial compression was done with a slow-speed wire saw using low loads to minimize damage. Prior to deformation, samples were heat-treated at 400 °C in a muffle furnace for 24–36 h and they were further subjected to variable intervals (of up to 24 h) at < 300 °C inside the gas-medium deformation apparatus. Dry commercial argon gas was used as the high pressure confining fluid in these deformation experiments. Although the isotopic content of this gas is not known, thick silver jackets isolated the mica samples from the confining fluid, and any contamination of the samples by this fluid would have been detected with the mass spectrometer. Jacket leaks during the experiments were not detected. Deformation experiments lasted for about 1.5 h. Further details of these deformation experiments are given in Mares and Kronenberg (1993).

Two splits of the undeformed Methuen muscovite single crystal were irradiated with neutrons and then step-heated to provide control on the amount of argon lost during deformation. Another split of the undeformed muscovite was irradiated and then crushed on-line with the mass spectrometer. The undeformed splits that were used for step-heating and crushing were not heat-treated in a muffle furnace prior to analysis.

The general procedures followed in $^{40}Ar/^{39}Ar$ dating of micas in this study are described in detail by Dunlap (1997); additional specifics are given here. The samples were irradiated for 120 h in a Ford reactor, University of Michigan, without cadmium shielding. Samples were stacked in single file in a silica tube (5 mm i.d.), with the neutron fluence monitor Fish Canyon Sanidine (27.8 Ma; Cebula et al. 1985) interspersed between samples at ~5-mm intervals. J-values for samples were determined by interpolation to be in the range 0.01957–0.01967 ± 0.3% for the Methuen muscovite and 0.01524 ± 0.3% for the single Fe-mica sample, with total variation along the length of the tube occupied by the samples (1 cm) of < 1%. During step-heating, sample temperature was monitored by a thermocouple at the base of a tantalum crucible within a double-vacuum resistance furnace. Experiments were started in the 400–550 °C range and concluded at 1,500 °C. Heating schedules are listed in the supplementary data tables; each heating step was for 10–25 min depending on the amount of gas desired for analysis.

At each extraction temperature, the gas released was exposed to Zr–Al getter pumps to remove active gases, and the argon was subsequently isotopically analyzed using a VG1200 gas-source mass spectrometer operated in the static mode. Measurements were made with an electron multiplier (with an Ar sensitivity of about 5×10^{-17} mol mV^{-1}). Getter section blanks were normally

below 5×10^{-16} mol on mass 40 for static collection over 10 min. Blanks were atmospheric, as well as could be determined, and the mass 39 blank (10 min) was normally below 2×10^{-18} mol. Furnace blanks below 1,000 °C were generally well below 5×10^{-15} mol of ^{40}Ar. The ^{40}K abundance and decay constants ($\lambda = 5.543\times10^{-10}$ a^{-1}) recommended by the IUGS Subcommission on Geochronology were used (Steiger and Jager 1977). Data were corrected for mass spectrometer discrimination, line blanks, and for the decay of ^{37}Ar and ^{39}Ar during and after irradiation. Amounts of ^{39}Ar listed in the supplementary data tables are derived from the measured sensitivity of the mass spectrometer (uncertainties of ~5%). Totals are the percent ^{39}Ar weighted means of the analyses. Correction factors for Methuen muscovite determined from irradiated salts are the following: $(40/39)_K = 0.025$; $(36/37)_{Ca} = 0.00026$; $(39/37)_{Ca} = 0.00072$; $(38/39)_K = 0.012$. For the Fe-mica these values are $(40/39)_K = 0.021$; $(36/37)_{Ca} = 0.00024$; $(39/37)_{Ca} = 0.00074$; $(38/39)_K = 0.012$. These factors have measured errors of $< \sim 5\%$, and thus little affect the outcome of the experiments.

Results

Fe-mica

The age spectrum for the undeformed split of the Fe-mica is somewhat erratic, not forming an ideal plateau, but it is essentially flat over the entire gas release, yielding an integrated weighted mean age of 307.2 ± 0.8 Ma (Fig. 2a); all ages quoted with one sigma uncertainty (results for all experiments are tabulated in supplementary database). This result is in agreement with the 307.6 ± 0.4 Ma weighted mean age determined by Grove and Harrison (1996) from eight total fusion measurements on aliquots of several milligrams of the Fe-mica.

A limited amount of gas was extracted from the aliquot of Fe-mica crushed on-line with the mass spectrometer. Using the measured sensitivity of the mass spectrometer, the weight of the crushed aliquot, and the argon concentration of the mica, we estimate that ~2.5% of the total available ^{39}Ar was released during crushing. The age spectrum of the crush release experiment (Fig. 2b) exhibits individual ages that range from 289 to 328 Ma. Although the age spectrum is markedly erratic, the integrated gas age is 307.3 ± 4.3 Ma, which is identical within uncertainty to that of the step-heat measurements of the undeformed material.

The four sieve fractions of the crushed Fe-mica were roughly equal in weight, with a total weight of 4.45 mg: < 25 μm (1.02 mg), 25–75 μm (1.22 mg), 75–150 μm (1.18 mg), and > 150 μm (1.03 mg). Some of the crushed material (1.05 mg) was "lost" in the sieving process. Step-heating of the < 25-, 25–75- and > 150-μm crushed fractions yielded age spectra with integrated weighted mean ages of 309.5 ± 1.3, 308.4 ± 0.9, and 305.9 ± 1.1 Ma, respectively. These integrated ages are within 1% of that determined for the undeformed material. The age spectra (Fig. 2c), however, are more variable than that of the undeformed material, with the two finest fractions yielding distinctly higher ages in the latter portion of gas release.

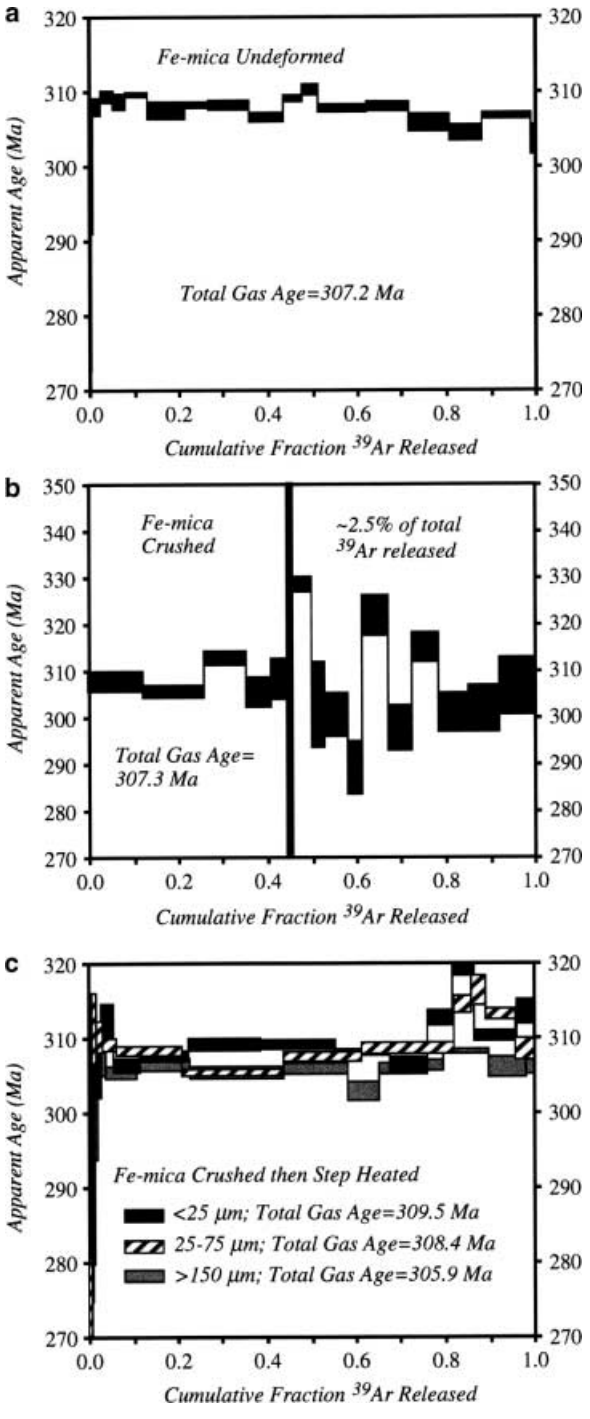

Fig. 2 ^{40}Ar/^{39}Ar age spectra for aliquots of Fe-mica. **a** Undeformed starting material, same as used by Grove and Harrison (1996). **b** Crush release from undeformed aliquot of Fe-mica comprising only ~2.5% of the available ^{39}Ar. **c** Age spectra for resized fractions of crushed Fe-mica: < 25, 25–75, and > 150 μm. The 75- to 150-μm-size fraction was not analyzed

Methuen muscovite

The Methuen muscovite specimen had an original size of at least 50 mm measured perpendicular to cleavage, and 45×90 mm within the cleavage (Mares and Kronenberg 1993). The cleavage section has the general shape of a rhombus. The two undeformed splits, designated M-A and M-B, were cut at ~1 and 2 cm from the margin of the crystal. M-B is a rectangular section, in the cleavage, measuring ~2.5×5mm (~120 μm thick), with minimum dimension in the cleavage of ~1,200 μm; M-A is an isosceles triangular section with 3 mm short dimension and 5 mm long dimensions in the cleavage, with minimum distance to geometric center in the cleavage of ~1,200 μm and a thickness of ~200 μm. The splits extracted for the deformation experiments of Mares and Kronenberg (1993) were extracted from the core of the crystal and the results below show that possible inhomogeneity in argon concentration is not an issue.

The step-heating analyses of undeformed splits M-A (4.69 mg) and M-B (4.25 mg) yield similar age spectra (Fig. 3a) with integrated ages of $1{,}043 \pm 1$ and $1{,}044 \pm 1$ Ma, respectively. Anomalously high ages are evolved in the first 10% of gas release in both cases, with a large fraction at ~1,386 Ma for M-A and one at ~1,098 Ma for M-B. The remainder of the gas release for both samples is essentially flat. For sample M-A a plateau age of $1{,}031 \pm 1$ Ma is formed by the last 77% of gas release (weighted mean age; i.e., all steps overlap with the weighted mean at the 2σ level). The result for sample M-B forms a plateau at $1{,}040 \pm 1$ Ma for the interval of 27–97% of gas release. These two age spectra are non-ideal in light of the observation that micas do not generally exhibit strongly elevated ages in the initial ~10% of gas release.

One split (4.54 mg) of the M-B undeformed muscovite was crushed on-line with the mass spectrometer (Fig. 3b). Using the measured sensitivity, the weight of the split, and the argon concentration of the step-heated split, we estimate that ~0.53% of the total available ^{39}Ar was released during crushing. The ages evolved during crushing declined continuously from 2,470–1,221 Ma and the amount of gas in each step increased as the torque on the crusher driver was increased to ~65 inch-pounds. The integrated age of the gas is ~1,381 Ma, which is ~33% older than the integrated age of the mica.

The modes of deformation and strain heterogeneity varied markedly in Methuen muscovite samples deformed in the triaxial deformation apparatus, depending on the crystallographic orientation of loading (Mares and Kronenberg 1993). Sample M-11, loaded at 45° to cleavage (and to [310]), was sheared by basal dislocation glide resulting in shear strains that are relatively homogeneous (Fig. 4a of Mares and Kronenberg 1993). Aliquots of 4.16 and 6.03 mg (measuring about ~1.5×4 mm rectangular in the cleavage; thicknesses ~250 and ~350 μm respectively) were extracted from the margin of the charge for step-heating. Sample M-22 was deformed in a similar geometry (though with a shear direction of [110]), and optical deformation microstructures are similar to those of M-11; some displacement may also have occurred on several cleavage surfaces, but pervasive dislocation slip is still believed to have been the predominant deformation mechanism at the confining pressure (200 MPa) imposed. A 5.35-mg

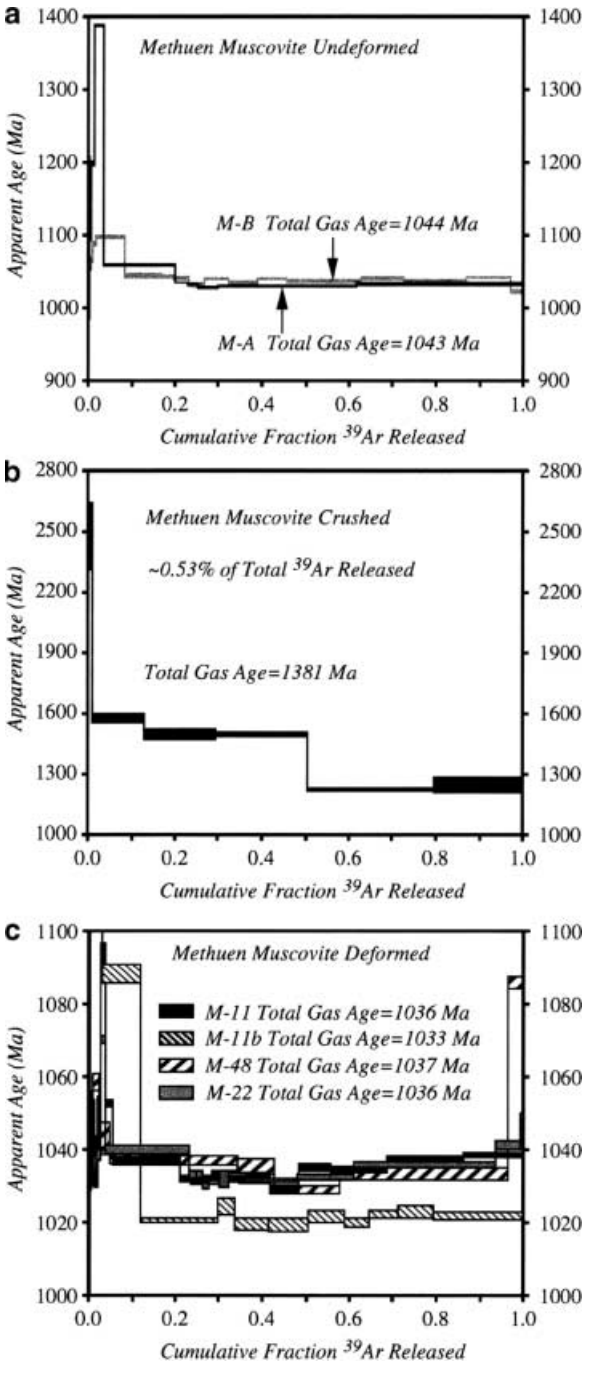

Fig. 3 ^{40}Ar/^{39}Ar age spectra for aliquots of Methuen muscovite. **a** Age spectra for two undeformed aliquots of the starting material; not heat treated. **b** Crush release from split of undeformed aliquot M-B; gas comprises only ~0.54% of the available ^{39}Ar. **c** Age spectra for sheared aliquots of Methuen muscovite deformed by Mares and Kronenberg (1993); samples are M-11, M-11b (a second split), M-22, and the kinked portion of M-48

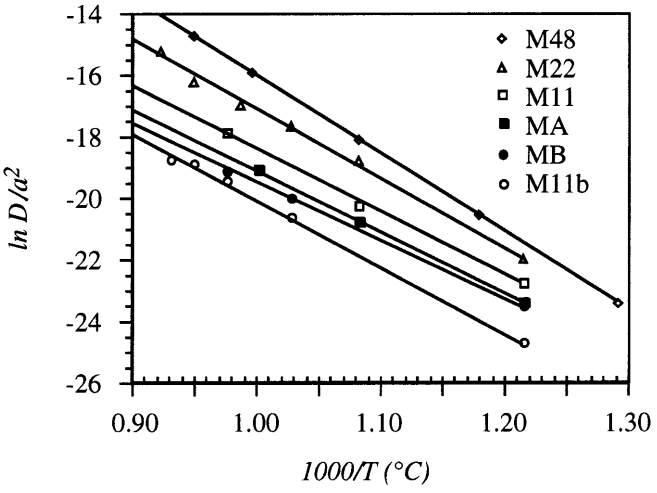

Fig. 4 Arrhenius plot of $\ln D/a^2$ versus reciprocal temperature for the step heat results for the six aliquots of Methuen muscovite

aliquot of the sample, measuring ~2×3 mm was extracted for step-heating (rectangular in the cleavage with one 2-mm edge forming the margin of the charge; thickness ~300 μm). The aliquot was extracted from a region of the charge away from any displaced cleavages (displaced segments indented the jacket). Sample M-48, loaded parallel to (001), experienced intense kinking at one end of the sample (Fig. 5a of Mares and Kronenberg 1993). Strains within much of this sample are negligible, whereas shear strains within the kinked material are much larger than implied by total sample shortening (of 11%). Deformation within the kinked regions involved dislocation slip parallel to cleavage and at least two generations of kink band formation accompanied by localized opening of cleavage cracks and development of sub-micron rhombohedral voids at kink band boundaries (Christoffersen and Kronenberg 1993; Mares and Kronenberg 1993). Kink band segmentation within this

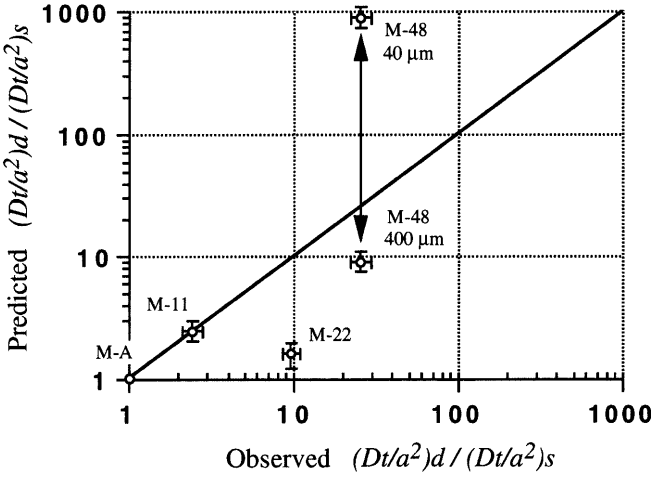

Fig. 5 Plot of predicted Dt/a^2 versus observed Dt/a^2 for the step heat results on Methuen muscovite at 650 °C

portion of the sample is intense with neighboring kink band boundaries defining domains of 2 μm to 400 μm in scale (Fig. 5b of Mares and Kronenberg 1993). A 4.80-mg aliquot of this kinked material was excavated for step-heating; the analyzed fragments are generally rectangular in the cleavage and they exhibit a grain size distribution similar to that shown in Mares and Kronenberg (1993, their Fig. 5b).

The four step-heating analyses of deformed Methuen muscovite samples – two from M-11 and one each from M-22 and M-48 – yield remarkably similar age spectra (Fig. 3c). These age spectra are also essentially indistinguishable from the step-heating measurements of the undeformed material; if they were plotted at the scale of Fig. 3a the age spectra would exhibit nearly continuous overlap. Anomalously high ages are exhibited in the first ~10% of gas release from the deformed samples. In addition, the M-48 spectrum exhibits a rise in age to 1,086 Ma in the last step (and we do not understand why). The two step-heating measurements of the M-11 muscovite are slightly different, the plateau-like portions differing by as much as 20 million years (M-11b plateau is younger by ~2%), and the initial elevated ages differing significantly in volume (that of M-11b is much larger). Nevertheless, the integrated ages of the two spectra measured for deformed sample M-11 are remarkably similar at 1,033 ± 1 (M-11b) and 1,036 ± 1 Ma (M-11), as are the M-22 and M-48 integrated ages of 1,036 ± 1 and 1,037 ± 1 Ma, respectively. In general, the integrated ages of the deformed Methuen muscovites are 0.7–1.0% below those of the undeformed samples. Radiogenic argon contents generally >90% indicate that exchange of argon between the mica starting material and atmospheric argon (or the argon confining fluid) was negligible during the deformation experiments.

Step-heating data are known to exhibit excess scatter on Arrhenius plots (McDougall and Harrison 1989) in comparison with isothermal hydrothermal data. Nevertheless, Arrhenius plots for the six heating experiments on Methuen muscovite exhibit excellent linear fits as diffusivity increases with increasing furnace temperature from ~500 to 810 °C (Fig. 4); D_o is the apparent diffusivity and a is the characteristic diffusion length scale. Errors in temperature are within the width of the symbols and a one sigma error in the log of diffusivity is less than one half of a log unit (e.g., Grove and Harrison 1996). At temperatures >~810 °C, the apparent diffusivities depart from the linear relationship, most likely because of the progressive breakdown of the samples by dehydroxylation and dehydration (Vedder and Wilkins 1969). For temperatures <810 °C, the samples yield activation energies ranging from 37.0–50.3 kcal mol^{-1}, which is about the range previously observed for muscovite, although higher activation energies seem to be preferred (e.g., Hames and Bowring 1994).

Samples were step-heated by similar, although not identical, temperature–time schedules. By 750 °C, the undeformed M-B muscovite had released only 0.56% of

its total ^{39}Ar whereas by ~750 °C the sheared muscovite aliquots M-22, M-11, and M-11b had released 1.7, 1.1, and 0.5%, respectively, and by 730 °C the heavily deformed sample M-48 had released ~2.6% of its total ^{39}Ar (by 780 °C M-48 had released 5.1%).

Although $^{40}Ar/^{39}Ar$ ages of the deformed Methuan muscovite samples are only slightly affected (0.7–1.0% level), apparent diffusivities of Ar determined from quantities of argon released during step-heating seem to be greater than determined for the undeformed starting material for three of the four deformed sample analyses (Fig. 4). The scatter expected from the step-heating method may account for the differences between the M-A, M-B, M-11, and M11b results. However, increases in apparent diffusivity are seen for the M-22 muscovite, of about two orders of magnitude, and the intensely kinked region of M-48 yields calculated D/a^2 values some 2.7 orders of magnitude greater than determined for the starting material ($\ln D/a^2 = -18.1$ for M-48 as compared with $\ln D/a^2 = -20.8$ for Methuan muscovite starting material).

Estimates of fractional loss

The most important consideration in this study is whether the bulk diffusivity of argon is increased by the introduction of dislocations and whether this can account for the results above. The simplest explanation of the apparent increase in diffusivity for M-48 would be that the diffusional distance has been severely reduced by kinking. One way to assess the possibility of increased diffusivity for the M-48 kinked material is to plot the data as log D versus $1/T$, using the minimum physical dimension in the cleavage between kink band boundaries as a. However, as the M-48 aliquot is composed of a wide range of kink band widths (~2–400 μm), such a plot is difficult to interpret. Run times vary as well, so times for diffusion are not exactly equal.

Another way of examining argon loss is to plot the observed Dt/a^2 versus predicted Dt/a^2 for an infinite cylinder, expressed as a ratio against that of the starting material at one temperature (Fig. 5). Grain size effects and differences in run times cancel out on this plot and the departure from theory should be obvious if the diffusivity does not vary systematically with the square of diffusion dimension. A reference value of Dt/a^2 was taken for undeformed sample M-A at T = 650 °C and ratios of Dt/a^2 (Predicted/reference and Observed/reference) are shown for samples M-11, M-22, and M-48. The "observed" value of Dt/a^2 for each deformed sample was calculated from the measured fractional losses using the approximation of Reichenberg (1953), and the predicted value was found from the relationship $(Dt/a^2)_d = (Dt/a^2)_s \times (A_s/A_d)^2$, where A is taken as the minimum physical crystal dimension in the cleavage and the subscripts s and d refer to starting material and deformed charge, respectively. The largest source of uncertainty for the predicted values is in the estimate of A, whereas that for the observed values is in the ability to measure fractional loss ($\pm < 0.5\%$, drift in machine sensitivity was $< 1\%$ during the course of the step-heating experiments, and cannot account for the consistent differences between measured bulk ages of deformed and undeformed aliquots).

While the measured aliquots vary considerably in shape, making the estimate of A problematic, we consider that the shortest distance within the cleavage is a reasonable estimate of the effective diffusion distance for argon escape, within ~10%, and the error bars for "predicted" values on Fig. 5 reflect this uncertainty. Our preferred values for A are 1,200, 750, 1,000, and 40 μm for samples M-A, M-11, M-22, and M-48, respectively. The value of A for the M-48 kinked material was estimated petrographically from 100 measurements on a split of the step-heated material, although it is clear that this very fine material represents a minor amount by volume and the ~400 μm material dominates the volume. The 1:1 line on Fig. 5 is where the data would plot if our fractional loss data corresponded exactly to loss from an infinite cylinder using the above values for A. Although observed values are equivalent to or exceed predicted values for M-11 and M-22, that for the kinked M-48 material is significantly lower than predicted, assuming the mean distance of 40 μm between kink band boundaries. If 400 μm is taken for the M-48 calculation, the observed and predicted values agree, plotting close to the 1:1 line. Thus, the fractional loss observed for the intensely kinked material of M-48 is not clearly enhanced over what we would expect from single domain diffusion. Note also that M-11b would plot to the left of the y-axis on this plot (see Discussion section where we speculate that this is because of refilling of dislocations, rather than diffusion directly out of the grain).

By projecting the linear fits on the Arrhenius plot back to 400 °C we can estimate the amount of argon that should have been lost via volume diffusion from samples during pretreatment in the muffle furnace and the subsequent deformation experiments. Using the approximation for fractional loss from an infinite cylinder (Reichenberg 1953), the projected D/a^2 from the Arrhenius plots, and the times of pretreatment and deformation, we estimate that 0.04% of the total argon should have been lost during pretreatment (using Arrhenius data for the starting material), and that $< 0.01\%$ should have been lost during the deformation experiments (using the Arrhenius relation fit to M-48 data), for a total of 0.05%. These estimates stand in contrast with the total gas ages of the deformed aliquots of Methuen muscovite, which are up to 1% younger than the untreated and undeformed starting material. The 1% reduction in age would seem to require ~20 times the loss expected from the above calculations.

Lee (1995) suggested that available hydrothermal diffusion data on micas is consistent with simultaneous multipath diffusion through both the mica lattice and extended defects such as dislocations, and there are some interesting arguments for multiple length scales of

diffusion in micas (e.g., Grove and Harrison 1996; Dunlap 1997). Lee (1995) estimates that diffusion of argon through dislocations could be faster than that through a mica lattice by more than 3–4 orders of magnitude. If we assume that the effective radius of a dislocation (including its core and a diffuse Cottrell atmosphere) is 100 Å and we take the observed maximum dislocation density of $\sim 5\times10^{6}$ mm^{-2} (Mares and Kronenberg 1993), we obtain a volume fraction for dislocations in deformed muscovite samples of 0.16% (50 Å gives 0.04% and 200 Å gives 0.63%), which is of the order of the amount of argon lost during the deformation experiments. Although the dislocation densities of naturally deformed micas are known for only a few localities (e.g., Wilson and Bell 1979), we do not expect densities of naturally deformed micas to exceed those of experimentally deformed samples in many cases, and volume fraction of anomalously high diffusivity surrounding dislocations is unlikely to be more than a few percent. We have modeled the argon loss from Methuen muscovite as a multipath diffusion problem, employing the Fortran program of Lee and Aldama (1992). Diffusional transport out of an infinite cylinder was examined using a frequency factor $D_0 = 10$ s^{-1} and activation energy 43 kcal mol^{-1} for volume diffusion; these values are suggested by the Arrhenius relation fit to the data for undeformed Methuen muscovite. For diffusion through the dislocations we chose the same value for D_0 as for volume diffusion, but assumed a smaller activation energy of 38 kcal mol^{-1}; these values predict a difference in diffusivity between the dislocations and the lattice of almost four orders of magnitude at 400 °C ($\ln D_0/a^2 = -21.5$ for dislocations and –25.2 for the lattice). For the multipath calculations, a number of additional parameters needed to be specified (see Lee and Aldama 1992; $\kappa_1 = 2\times10^{-15}$ s^{-1}; $\kappa_2 = 1\times10^{-15}$ s^{-1}; $c_1 = c_2$ or $c_2 = 1$, $c_1 = 0$) depending on whether dislocations are filled with or empty of the diffusing species. For the run conditions and the parameters cited above, the multipath model predicts that the loss of ^{40}Ar during the relatively brief deformation experiments at 400 °C, added to the loss by volume diffusion during heat pretreatment, should be $\sim$1%. Although the model parameters are only our best guesses, and we might have used a more retentive model for volume diffusion (e.g., Hames and Bowring 1994), it is clear from our calculations that the 1% loss of argon that we observe for the deformed Methuen muscovite requires the existence in our samples of fast diffusion pathways where argon diffusion is several orders of magnitude faster than volume diffusion at 400 °C.

Discussion

Not all processes involved in natural deformations of micas are replicated in our experiments, nor can we expect to simulate diffusive transport in experimental time scales with the same relative rates of volume and pipe diffusion as are important in the Earth. Nevertheless, the results of our experiments may be applicable to some natural situations and provide constraints on the effect that deformation might have on the argon age of micas. The crushing experiments performed on biotite most closely approximate cataclastic deformations, with the production of numerous cleavage-perpendicular cracks, accompanied by the glide motion of dislocations and propagation of cracks along the cleavage at conditions that preclude any thermally activated argon loss through the lattice. The triaxial compression of muscovite single crystals has resulted in undulatory extinction and the development of kink bands reminiscent of microstructures observed in micas deformed under greenschist facies conditions, though in the absence of recrystallization. We anticipate that the deformation in these experiments provides a close analog to deformation of muscovite under greenschist facies conditions and can be used to separate the importance of slip-induced argon loss from changes in argon content associated with recrystallization and resultant changes in diffusion length scales. The principal shortcoming of these experiments involves the short time scale of the laboratory deformations.

The results of crushing Fe-mica are not difficult to interpret. Although the crush release spectrum is markedly erratic (consistent with differential siting of ^{40}Ar and ^{39}Ar), and the step-heating of the crushed material yields non-ideal age spectra, the integrated ages of these experiments are essentially indistinguishable from that of the undeformed material. The slightly elevated ages near the end of step-heating of the two finest crushed fractions is worth noting, but we would prefer to run further experiments rather than speculate on their significance. The broad conclusion from the crushing of Fe-mica is that no significant argon has been lost in the crushing process. The implication for cataclasis of micas in low temperature natural environments is that argon loss during mechanical grain size reduction, resulting directly from the deformation process, is not significant. Therefore, the mechanisms responsible for positive correlations between grain size and age in natural, cataclastically deformed mica populations are likely to be either (1) diffusive loss of argon over shorter distances following mechanical grain size reduction, and/or (2) chemically driven neocrystallization, in which new fine mica grains are introduced, leading to increased mica contents and populations with mixed ages.

The results of the triaxial compression experiments on muscovite are somewhat more difficult to interpret. The bulk ages of the undeformed and deformed muscovites that were step-heated are distinguishable at the 1% level and the plateau-like portions of the six experiments range $< 2\%$. This indicates that the level of argon lost during the course of the deformation experiments is at the limit of resolution of typical dating studies. However, the deformed muscovite samples yield systematically lower bulk ages, suggesting a slight enhancement of argon loss during deformation. The slightly lower argon concentration in the deformed

samples might be attributed to some contribution of relatively rapid pipe diffusion along dislocation networks. This possibility is supported by our estimate that only ~0.05% of the total ^{40}Ar should have been lost by volume diffusion during the heat treatments prior to (at 400 °C for 24–36 h in a muffle furnace and ~300 °C for ~24 h) and during deformation (400 °C for 1.5 h). In contrast, the multipath model, which combines volume diffusion and fast pathway diffusion in parallel, predicts ~1% loss of ^{40}Ar for the run conditions.

Is it possible to draw conclusions from our data regarding segregation of argon impurities at dislocations and enhanced mobilities in Methuen muscovite? The challenge is to reconcile the Arrhenius data, the form of the age spectra, the 1% loss of ^{40}Ar prior to the step heating experiments, the similarity of the Arrhenius relations for deformed and undeformed aliquots, and the observation that loss was enhanced over volume diffusion by a factor of up to ~20.

Activation energies for pipe diffusion are generally smaller than those for volume diffusion (Balluffi 1970; Yund et al. 1981; Ho and Pratt 1983; Wolfenstine 1990; Sakaguchi et al. 1992) and an increase in the contribution of pipe diffusion should lead to reduced values for bulk multipath diffusion. However, unless the net transport along dislocations becomes very large, apparent activation energies of bulk diffusion rates are not expected to be reduced very much below that of lattice diffusion (Shewmon 1963; Yund et al. 1981). No such change is evident from our Arrhenius plots of argon released during step-heating (Fig. 4); instead, activation energies for the deformed samples (41.0–50.3 kcal mol^{-1}) would appear to be the same as or greater than values for the undeformed samples (37.0 and 40.2 kcal mol^{-1}). Thus, under conditions of the step-heating analyses ($T > 450$ °C), pipe diffusion does not appear to contribute significantly to the overall argon loss, at least as reflected in the form of the Arrhenius data.

This conclusion may or may not hold at the conditions of the deformation experiments ($T = 400$ °C). The ~1% reduction in ^{40}Ar prior to step-heating analyses suggests that a small fraction of the total argon may have been lost by way of mobile dislocations. At lower temperatures, the difference between diffusion coefficients along dislocations and within the lattice is expected to increase, which may lead to extensive drainage of argon from dislocation networks while argon concentrations of the lattice remain little changed. In addition, argon loss may have been facilitated during the deformation experiments by the active slip of dislocations, increasing the effective volume fraction of the mica grains that dislocations are able to deplete. Dislocation motions during hydrostatic step-heating, associated with any recovery of dislocations into stable configurations, were probably very limited.

The elevated ages of the initial steps during heating of both the deformed and undeformed Methuen muscovite are derived from gas that is loosely held relative to the bulk of the radiogenic argon. This behavior is not often seen in micas, but in other minerals such as K-feldspars and amphiboles it is indicative of excess radiogenic argon contamination. The anomalously high ages evolved during the crushing experiment on the undeformed split of the muscovite would seem to confirm the presence of excess argon. One test for excess argon contamination is to check for positive correlation between elevated ages and chlorine-derived ^{38}Ar. However, plots of $^{40}Ar^*/K$ versus Cl/K (Turner and Wang 1992) for the Methuen muscovite samples do not reveal any correlation. It may be that the elevated ages in the initial gas release result from lattice damage during sample preparation; however, the results for crushing and step-heating of the Fe-mica do not support this possibility; the initial stages of gas release during Fe-mica step-heating experiments reveal only slightly elevated ages relative to the plateau. An alternative possibility is that loosely held ^{40}Ar in Methuen muscovite is released from defects during both crushing and the early stages of step-heating, from sites that are otherwise devoid of K–Ca–Cl-bearing phases from which argon isotopes might be derived during irradiation. We speculate that this loosely held component of ^{40}Ar resides at defects and that it was accessed preferentially during the deformation experiments. During step-heating of the undeformed aliquots this component was accessed in excess over ^{39}Ar that had recoiled into more retentive sites.

The age spectra for deformed Methuen muscovite suggest that the loosely held component of ^{40}Ar (age spikes, first ~15% of gas) is markedly reduced relative to that in the undeformed mica. The loss of this component during deformation and heat pretreatment can account for the observed 0.7–1.0% reduction in age of the deformed aliquots. The possibility that dislocations have accessed this component and acted to remove it from the deformed aliquots is appealing, but how then do we explain the dramatic age spike for M-11b? This loosely held component of ^{40}Ar in sample M-11b is the most dramatic age spike of the deformed samples. Note also, however, that the plateau-like segment of M-11b is distinctly lower (~1.5%) than that of the other deformed aliquots and that is also has the lowest integrated age. If a loosely held component of argon was released from dislocations and other defects and lost during the heat pretreatment and deformation of M-11b, we may speculate that these sites became refilled with argon (a second loosely held component) from the lattice during the initial stages of step-heating. When the mica dehydroxylated at 880 °C the lattice-derived argon that refilled the defective sites was lost in a burst. This lost fraction of lattice-derived argon was then not able to contribute to the plateau-like segment of the age spectrum, thus, the ~1.5% reduction in plateau-like age.

The Arrhenius data and the age spectra for the deformed and undeformed aliquots of Methuen muscovite indicate that deformation-related argon loss is minor, in dating terms. Yet, the consistency between observed (0.7–1.0%) and expected (multipath model) loss of ^{40}Ar due to heat pretreatment and deformation, and the

possibility that argon loss was enhanced over volume diffusion by a factor of ~20, are all consistent with the possibility that argon has been partitioned into dislocations and other extended defects during deformation, and then lost from the grains via rapid pipe diffusion. In all fairness, however, we must emphasize that this evidence, although compelling, is still circumstantial.

Conclusions

$^{40}Ar/^{39}Ar$ dating of micas deformed (1) by crushing cataclastically at room temperature on-line (under vacuum) in a mass spectrometer and (2) by loading in triaxial compression at T = 400 °C (and confining pressures of 100 and 200 MPa) in orientations favoring dislocation slip and kinking failed to reveal any major changes in age from those determined for the mica starting materials. Although time scales for deformation differ in the laboratory and in nature, these results provide constraints on direct effects of deformation processes on age resetting of micas. Argon loss by purely mechanical processes of cataclasis in the natural environment is likely to be insignificant, as it is in the laboratory. Thus, positive correlations observed between grain size and age in natural cataclastically deformed mica populations are most likely caused by (1) diffusive loss of argon after mechanical grain size reduction, and/or (2) growth of new grains of mica driven by chemical driving forces (e.g., neocrystallization), augmenting the overall mica population and leading to mixed ages.

The percent level argon loss observed in our experiments, and the fact that this component is loosely held ^{40}Ar (in excess over ^{39}Ar) suggests that argon was partitioned into defective sites in the natural environment, accessed preferentially by moving dislocations during the deformation experiments and lost from the grains via rapid pipe diffusion. However, argon loss from white micas undergoing dislocation slip within the K-interlayer and/or kinking under greenschist facies conditions, either by processes of pipe diffusion or solute segregation at mobile dislocations (and resultant solute sweeping), is likely to be limited, and significant changes in argon ages are not expected. Diffusional argon loss during the initial stages of step-heating analyses following the triaxial compression experiments suggest that closure temperatures of intensely sheared and kinked micas may be somewhat lower than those of undeformed, but otherwise identical micas. The ability of experimentally sheared and kinked micas to retain argon is reduced primarily by reductions in the characteristic diffusion dimensions associated with the introduction of kink band boundaries, and to a lesser extent by modest contributions of pipe diffusion to net transport. We conclude that the most significant role of deformation to the argon ages of micas in natural mylonites and shear zones is in grain segmentation and grain size refinement, reducing the length scales for volume diffusion, and/or contributing to the nucleation of new mica grains. We speculate that the wide range of deformation features observed within individual porphyroclasts may affect the ability to retain argon, such that the porphyroclasts are likely to contain age gradients that correlate spatially with their deformation features. This may provide an explanation for the markedly rising age spectra of aggregates of internally deformed micas.

Acknowledgements Laboratory facilities were freely provided by Prof. Mark Harrison (UCLA). This study benefited significantly from discussions with Matt Heizler and Marty Grove. Dunlap wishes to thank the National Science Foundation for generous salary support while at the University of California, Los Angeles as an NSF Postdoctoral Fellow, and Kronenberg thanks the National Science Foundation for support under grant EAR-8816283.

References

Arabczyk W, Militzer M, Mussig H-J, Wieting J (1988) Contribution of pipe diffusion to surface segregation kinetics. Surface Sci 198:167–179

Badrour L, Moya EG, Bernardini J, Moya F (1989) Fast diffusion of silver in single and polycrystals of a-alumina. J Phys Chem Solids 50:551–561

Balluffi RW (1970) On measurements of self-diffusion rates along dislocations in FCC metals. Phys State Solid 42:11–34

Banos JO, Amouric M, De Fouquet C, Baronnet A (1983) Interlayering and interlayer slip in biotite as seen by HRTEM. Am Mineral 68:754–758

Behrmann JH (1984) A study of white mica microstructure and microchemistry in a low grade mylonite. J Struct Geol 6:283–292

Bell IA, Wilson CJL (1981) Deformation of biotite and muscovite: TEM microstructure and deformation model. Tectonophysics 78:201–228

Bell IA, Wilson CJL, McLaren AC, Etheridge MA (1986) Kinks in mica: role of dislocations and (001) cleavage. Tectonophysics 127:49–65

Borg I, Handin J (1966) Experimental deformation of crystalline rocks. Tectonophysics 3:249–368

Cebula GT, Kunk MJ, Mehnert HH, Naeser CW, Obradovich JD, Sutter JF (1985) The Fish Canyon Tuff, a potential standard for the $^{40}Ar/^{39}Ar$ and fission track dating methods. Terra Cognita 6:139

Chen I-W (1984) Anisotropic diffusion of point defects to edge dislocations. J. Nucl Mater 125:52–63

Christoffersen R, Kronenberg AK (1993) Dislocation interactions in experimentally deformed biotite. J Struct Geol 15:1077–1095

Cottrell AH, Jaswon MA (1949) Distribution of solute atoms round a slow dislocation. Proc R Soc Lond 199:104–114

Demny J (1963) Elektronenmikroskopische Untersuchungen an sehr dunnen glimmer Folien. A. Naturforsch A18a:1088–1096, 1097–1101

Dodson MH (1973) Closure temperature in cooling geochronological and petrological systems. Contrib Mineral Petrol 40:259–274

Dunlap WJ (1997) Neocrystallization or Cooling?: $^{40}Ar/^{39}Ar$ ages of white micas from low grade mylonites. Chem Geol 143:181–203

Dunlap WJ, Teyssier C, McDougall I, Baldwin S (1991) Ages of deformation from $^{40}Ar/^{39}Ar$ dating of white micas. Geology 19:1213–1216

Dunlap WJ, Teyssier C, McDougall I, Baldwin S (1995) Thermal and structural evolution of the intracratonic Arltunga Nappe Complex, central Australia. Tectonics 14:1182–1204

Estrin Y, Rabkin E (1998) Pipe diffusion along curved dislocations: an application to mechanical alloying. Scripta Mater 39:1731–1736

Etheridge MA, Hobbs BE, Paterson MS (1973) Experimental deformation of single crystals of biotite. Contrib Mineral Petrol 38:21–36

Friedel J (1964) Dislocations. Pergamon Press, Oxford

Goodwin LB, Renne PR (1991) Effects of progressive mylonitization on Ar retention in biotites from the Santa Rosa Mylonite Zone, California, and thermochronologic implications. Contrib Mineral Petrol 108:283–297

Goodwin LB, Wenk H-R (1990) Intracrystalline folding and cataclasis in biotite of the Santa Rosa mylonite zone: HVEM and TEM observations. Tectonophysics 172:201–214

Grove M, Harrison TM (1996) $^{40}Ar^{*}$ diffusion in Fe-rich biotite. Am Minerol 81:940–951

Gukasyan A, Kvit A, Klevkov Y, Oktyabrsky S (1996) High-resolution PL characterization of impurity segregation and their complex formation on extended defects in CdTe. Solid State Commun 97:897–902

Gusev GM, Arkhipenko DK, Doil'nitsyn EF, Klyarovskiy VM (1969) Effect of ultrafine grinding on micas and their argon content. Geochem Int 6:80–88

Hames WE, Bowring SA (1994) An empirical evaluation of the argon diffusion geometry in muscovite. Earth Planet Sci Lett 124:161–167

Hames WE, Cheney JT (1997) On the loss of $^{40}Ar^{*}$ from muscovite during polymetamorphism. Geochim Cosmochim Acta 61:3863–3872

Hanson GN, Gast PW (1967) Kinetic studies in contact metamorphic zones. Geochim Cosmochim Acta 31:1119–1153

Hara K, Endo T (1997) Numerical approach to the I-S effect in ferritic heat-resisting steels. Mater Sci Eng A234:234–236

Harrison TM, Heizler MT, Lovera OM (1993) In vacuo crushing experiments and K-feldspar thermochronology. Earth Planet Sci Lett 117L:169–180

Hart EW (1957) On the role of dislocations in bulk diffusion. Acta Metall 5:597

Ho YK, Pratt PL (1983) Dislocation pipe diffusion in sodium chloride crystals. Radiat Effects 75:183–192

Hurlbut CS Jr (1956) Muscovite from the Methuen Township, Ontario. Am Mineral 41:892–898

Itaya T, Takasugi H (1988) Muscovite K–Ar ages of the Sanbagawa schists, Japan and argon depletion during cooling and deformation. Contrib Mineral Petrol 100:281–290

Kelley S (1988) The relationship between K/Ar mineral ages, mica grain sizes and movement on the Moine thrust zone, NW Highlands, Scotland. J Geol Soc Lond 145:1–10

Kligfield R, Hunziker J, Dallmeyer RD, Schamel S (1986) Dating of deformation phases using K–Ar and $^{40}Ar/^{39}Ar$ techniques: results from the Northern Appenines. J Struct Geol 8:781–798

Kronenberg AK, Kirby SH, Pinkston J (1990) Basal slip and mechanical anisotropy of biotite. J Geophys Res 95:19257–19278

Kronenberg AK, Mares VM, Christoffersen RG (1992) Deformation of micas: easy glide and effects of crystal chemistry and structure on (001) dislocation motion. EOS Trans Am Geophys Union 73:528

Le Claire AD, Rabinovitch A (1984) The mathematical analysis of diffusion in dislocations. In: Murch GE, Nowick AS (eds) Diffusion in crystalline solids. Academic Press, London, pp 257–318

Lee JKW (1995) Multipath diffusion in geochronology. Contrib Mineral Petrol 120:60–82

Lee JKW, Aldama AA (1992) Multipath diffusion: a general numerical model. Comput Geosci 18:531–555

Leonesio RB (1968) An observation made on the fracture properties of mica. Eng Fract Mech 1:237–238

Lister GS, Snoke AW (1984) S–C mylonites. J Struct Geol 6:617–638

Mares VM, Kronenberg AK (1993) Experimental deformation of muscovite. J Struct Geol 15:1061–1075

McDougall I, Harrison TM (1988) Geochronology and thermochronology by the $^{40}Ar/^{39}Ar$ method. Oxford University Press, New York

Meike A (1989) In situ deformation of micas: a high voltage electron microscope study. Am Mineral 74:780–796

Noe DC, LaVan DA, Veblen DR (1999) Lap shear testing of biotite and phlogopite crystals and the application of interferometric strain/displacement gages to mineralogy. J Geophys Res 104:17811–17822

Obreimoff JW (1930) The splitting strength of mica. Proc R Soc Lond Ser A 127:290–297

Reddy SM, Potts GJ (1999) Constraining absolute deformation ages: the relationship between deformation mechanisms and isotope systematics. J Struct Geol 21:1255–1265

Reichenberg D (1953) Properties of ion-exchange resins in relation to their structure: III. Kinetics of exchange. Am Chem Soc J 75:589–597

Ruoff AL, Balluffi RW (1963) Strain-enhanced diffusion in metals. II. Dislocations and grain-boundary short-circuiting models. J Appl Phys 34:1848–1853

Sakaguchi I, Yurimoto H, Sueno S (1992) Self-diffusion along dislocations in single-crystal MgO. Solid State Commun 84:889–893

Scaillet S, Feraud G, Ballevre M, Amouric M (1992) Mg/Fe and [(Mg,Fe) Si–Al_2] compositional control on argon behaviour in high-pressure white micas: $A^{40}Ar/^{39}Ar$ continuous laser-probe study from the Dora–Maira nappe of the internal western Alps, Italy. Geochim Cosmochim Acta 56:2851–2872

Shea WT, Kronenberg AK (1992) Rheology and deformation mechanisms of an isotropic mica schist. J Geophys Res 97:15201–15237

Shewmon PG (1963) Diffusion in solids. McGraw-Hill, New York, p 178

Shiryaev SY, Nylandsted Larsen A, Safronov N (1989) Rapid thermal annealing of indium-implanted silicon single crystals. J Appl Phys 65:4220–4224

Steiger R, Jaeger E (1977) Subcommission on geochronology: convention on the use of decay constants in geo- and cosmochronology. Earth Planet Sci Lett 36:359–362

Suprun IT (1982) Forced pipe diffusion of mobile pinning points. Phys State Solid A 74:411–419

Turner G, Wang S (1992) Excess argon, crustal fluids and apparent isochrons from crushing of K-feldspars. Earth Planet Sci Lett 110:193–211

Varschavsky A, Donoso E (1997) Modelling the kinetics of solute segregation to partial dislocations for isothermal microcalorimetric evaluations. J Thermal Anal 50:533–545

Vedder W, Wilkins RWT (1969) Dehydroxylation and rehydroxylation, oxidation and reduction of micas. Am Miner 54:482–509

West DP, Lux DR (1993) Dating mylonitic deformation by the ^{40}Ar-^{39}Ar method: an example from the Norumbega Fault Zone, Maine. Earth Planet Sci Lett 120:221–237

Wilson CJL (1980) Shear zones in a pegmatite: a study of albite–mica–quartz deformation. J Struct Geol 2:203–209

Wilson CJL, Bell IA (1979) Deformation of biotite and muscovite: optical microstructure. Tectonophysics 58:179–200

Wolfenstine J (1990) Effects of pipe diffusion on the creep behavior of dry olivine. Philos Mag 62:233–238

Yund RA, Smith BM, Tullis J (1981) Dislocation-assisted diffusion of oxygen in albite. Phys Chem Mineral 7:185–189

Yund RA, Quigley J, Tullis J (1989) The effect of dislocations on bulk diffusion in feldspars during metamorphism. J Metamorph Geol 7:337–341

Yurimoto H, Morioka M, Nagasawa H (1989) Diffusion in single crystals of melilite: I. oxygen. Geochim Cosmochim Acta 53:2387–2394

Yurimoto H, Morioka M, Nagasawa H (1992) Oxygen self-diffusion along high-diffusivity paths in forsterite. Geochem J 26:181–188